e-ISSN: 2550-164X

Available online at
https://jmeche.uitm.edu.my/

Journal of Mechanical Engineering 22(1) 2025, 118 – 136.

Journal of Mechanical Engineering

Direct Integration Mode Superposition: A Simple Method for Dynamic Analysis of Submerged Floating Tunnel (SFT)

Jamiatul Akmal[1*], Nurcahya Nugraha[1], Asnawi Lubis[1], Martinus[1]

[1]*Department of Mechanical Engineering, Universitas Lampung, Bandar Lampung, 35145, Indonesia*

ARTICLE INFO

Article history:
Received 4 April 2024
Revised 29 October 2024
Accepted 7 November 2024
Online first
Published 15 January 2025

Keywords:
Direct integration
Mode superposition method
SFT
Dynamic analysis

DOI:
10.24191/jmeche.v22i1.4559

ABSTRACT

This article describes the use of simple methods to analyze the dynamic behavior of large-dimensional structures, such as submerged floating tunnels (SFT). Using this method the calculation process becomes simple and inexpensive because the solution can be obtained analytically. Based on the superposition mode method, it is possible to directly integrate the Euler-Bernoulli beam theory model, which is called the Direct Integration-Mode Superposition Method (DI-MSM). Using Hamilton's principle, the equation of motion in the Euler-Bernoulli Beam model is modified into the Equation of forced damped vibration. The solution of the equation is obtained by direct integration to obtain the displacement and natural frequency. Evaluation of the effectiveness of this method was confirmed by solutions using FEM as validated with previous studies. This method is simpler to be applied in analyzing other structures, especially continuous structures with large dimensions, which if using the FEM method will require relatively large computational costs and longer time.

INTRODUCTION

A submerged floating tunnel (SFT) is a technology suitable for wide and deep strait crossings. The SFT is placed below the surface of the water at a certain depth and tied to the seabed by mooring cables. SFT is in the balance between buoyancy, construction weight, and tension in the mooring cable. For a wide crossing, the use of SFT is cheaper than a suspension bridge (Martire et al., 2010; Minoretti et al., 2016). SFT can also be used as an alternative to underground tunnels if the strait is a volcanic area that has the potential for earthquakes (Jin & Kim, 2021; Xiong et al., 2022).

The majority of previous studies on SFT used the finite element method (FEM), including for modal analysis (Muhammad et al., 2017; Sorokin et al., 2022; Kocakaplan & Tassoulas, 2019), dynamic response analysis for SFT due to fluid-vehicle-tunnel interaction (Lin et al., 2018; Yuan et al., 2016), and analysis of the influence of design parameters for SFT (Chen et al., 2018; Long et al., 2009; Mazzolani & Barbella, 2008). In addition, the FEM method is commonly used to analyze the effect of SFT depth level on dynamic response (Paik & Chang, 2004), analysis of the interaction between fluid flow and SFT structure (Remseth et al., 1999; Yu et al., 2020), and dynamic response of SFT due to seismic loads (Jin & Kim, 2018; Martinelli et al., 201; Xiong et al., 2023).

[1*] Corresponding author. *E-mail address*: jamiatul.akmal@eng.unila.ac.id
https://doi.org/10.24191/jmeche.v22i1.4559

The problem with using the FEM method is to analyze relatively large SFT structures and complexes that cause high computational costs and long computational times (Ereiz et al., 2021, 2022). In the FEM method, the numerical approach is usually derived from the cubic polynomial equation. The solution is obtained by integration, whose number of steps is proportional to the number of elements. The accuracy of the solution is also directly proportional to the number of elements used. A large number of elements results in a longer computational time. Thus, the FEM method is only effective for a small number of elements (Bathe, 2014) and is not effective for use in the analysis of relatively large SFTs.

To overcome the weaknesses of the FEM method, this study proposes to use the mode superposition method (MSM). In the original MSM method, space (x) and time (t) domains are used, which analytical solutions are difficult to solve. In this paper, we propose the Direct Integration-Mode Superposition Method (DI-MSM) as a solution, which is developed to be relatively simple and cost-effective in terms of computational expenses. The solution of the time domain (t) is solved numerically by direct integration. Thus, the overall solution of the modified MSM method is semi-analytic.

The SFT model, which is modeled as a beam on elastic support (BOES), is numerically modified to be a beam on elastic foundation (BOEF) (Sato et al., 2007; Sato et al. 2008). SFT is analogous to BOEF, which can simplify the analysis so that the eigenvalues (natural frequency and vibration mode) can be obtained easily. One example of using the MSM is for dynamic analysis of SFT under moving loads (Tariverdilo et al., 2011; Xiang et al., 2021). Previous research usually modeled SFT as an Euler-Bernoulli beam, and its dynamic solution can be solved by MSM (Rao, 2017b). In addition, the MSM method can also be used on dynamic multi-degree-of-freedom problems and continuous systems (Akgün, 1993; Thomson, 2018).

The present study analyzed the dynamic response to the SFT model with DI-MSM. As a comparison, analysis was also carried out with FEM. The hydrodynamic force caused by waves refers to the Morison Equation, which consists of a combination of drag and inertia forces. The SFT model is simplified by assuming that it is like a beam on an elastic foundation (BOEF). The differential equations in FEM and DI-MSM are both solved numerically using the Newmark method. This method is expected to provide an effective solution to describe the dynamic response of SFT, including the influence of parameters in the design.

This method will be applied to a case study example for SFT design in Qiandao Lake, China (Muhammad et al., 2017). The solutions studied include vibration mode, hydrodynamic force, displacement, and bending moment. In addition to being compared with the FEM method, these solutions are also in accordance with previous research (Muhammad et al., 2017). By using the DI-MSM, it is easy and fast to analyze the effects of design parameters, including the effect of the SFT depth level, the effect of the angle of the mooring cable, and the distance between the mooring cables.

METHODOLOGY

SFT modelling and analysis

The SFT has mooring cables attached at an angle of inclination (θ), and is arranged symmetrically along the longitudinal axis. The mooring cables are always in tension to balance the buoyancy. Fig 1 shows the SFT model in Cartesian coordinates. The direction of the hydrodynamic force is assumed to be parallel to the y-axis. The hydrodynamic force of the waves on the mooring cables is negligible because their diameter is very small compared to the diameter of the SFT.

https://doi.org/10.24191/jmeche.v22i1.4559

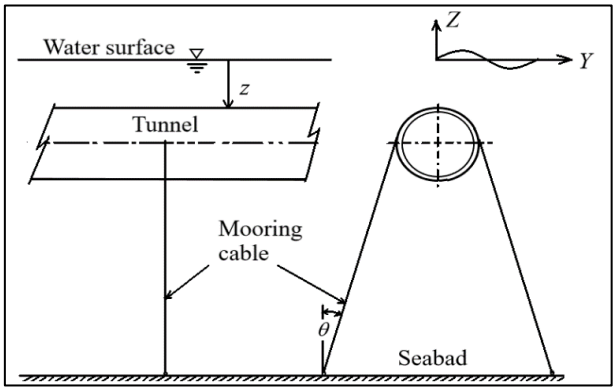

Fig. 1. SFT model and movement in cartesian coordinates (Sorokin et al., 2022).

The SFT equation of motion is formulated based on the Euler-Bernoulli beam theory, as shown in Fig 2. It is assumed that the SFT is supported simply so that the stiffness is only obtained from the flexural rigidity. It is also assumed that the length of the SFT is very large compared to the cross-sectional size, the displacement is small, and the rotational inertia and the shear deformation are neglected (Rao, 2017a). Its motion can be expressed by fourth-order parabolic partial differential equations as shown in Equation (1) (Rao, 2017a). In this equation, w is the displacement, EI is the flexural stiffness, ρA is mass per unit length and $f(x,t)$ is the hydrodynamic force.

$$\mathrm{EI}\frac{\partial^4 w}{\partial x^4}(x,t) + \rho A \frac{\partial^2 w}{\partial t^2}(x,t) = f(x,t) \tag{1}$$

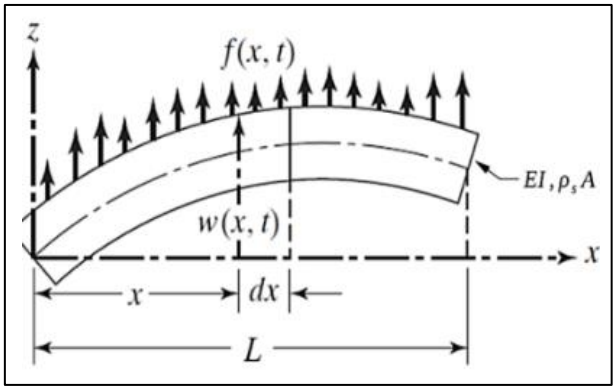

Fig. 2. Euler-Bernoulli Beam Model (Rao, 2017a).

Development of direct integration-mode superposition method (DI-MSM)

SFT can be modeled using the Euler-Bernoulli Beam equation, as shown in Equation (1). To obtain an analytical solution of this equation requires relatively high effort (Maqbul & Gupta, 2021; Tang & Karpov, 2014). DI-MSM is a relatively easy technique and requires little effort to solve the Euler-Bernoulli Beam equation (Blaszczyk, 2017). DI-MSM solves Equation (1) by converting it into an equation of motion in the form of an ordinary differential equation (ODE). In the first step, natural frequencies and mode shapes of SFT are determined by solving the eigenvalue problem. The original partial differential equation is

https://doi.org/10.24191/jmeche.v22i1.4559

converted into a set of ordinary differential equations (ODE) in terms of time-dependent coefficients, then solved with the direct integration method for each mode shape. The final step is superposition by combining the contributions from all modes to obtain the total response of the SFT. The steps of solving the equation of motion of SFT can be seen in Fig 3.

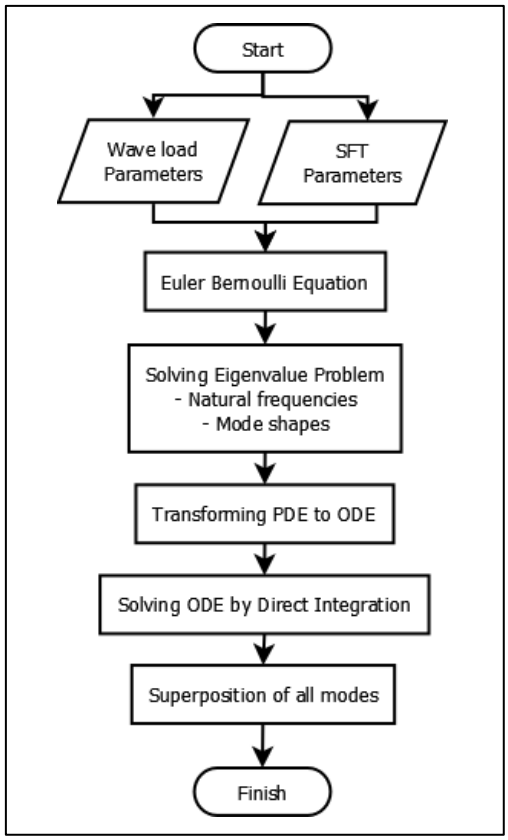

Fig. 3. DI-MSM steps to solve the equation of motion of SFT.

Using Hamilton's principle, in a more complete form, Equation (1) can be expressed as Equation (2) (Lin et al., 2019), where *m* is the sum of the structural mass and the added mass, *c* is the viscous damping, and *k* is the stiffness of the mooring cable.

$$EI\frac{\partial^4 w}{\partial x^2} + m\frac{\partial^2 w}{\partial t^2} + c\frac{\partial w}{\partial t} + kw = f(t) \tag{2}$$

The solution of Equation (2) using the MSM is obtained by expressing the dynamic response of the SFT as a superposition of the normal mode (Rao, 2017a), and the displacement is expressed by Equation (3).

$$w(x,t) = \sum_{n=1}^{\infty} W_n(x) q_n(t) \tag{3}$$

https://doi.org/10.24191/jmeche.v22i1.4559

Here $W_n(x)$ is the normal mode at the n^{th} vibrating mode and $q_n(t)$ is a function of time. Normal mode $W_n(x)$ depends on the type of boundary conditions of the SFT, in this study used SFT with simply supported beam boundary conditions with a pin support at both ends. Thus, the mode of vibration is as shown in Equation (4). If Equation (3) is substituted into Equation (2), Equation (5) will be obtained. The harmonic free vibration is as shown in Equation (6).

$$W_n(x) = sin\left(\frac{n\pi x}{L}\right) \tag{4}$$

$$EI\sum_{n=1}^{\infty}\frac{d^4W_n(x)}{dx^4}q_n(t) + m\sum_{n=1}^{\infty}W_n(x)\frac{d^2q_n(t)}{dt^2} + c\sum_{n=1}^{\infty}W_n(x)\frac{dq_n(t)}{dt} + k\sum_{n=1}^{\infty}W_n(x)\,q_n(t) = f(t) \tag{5}$$

$$EI\frac{d^4W(x)}{dx^4} = m\omega^2W(x) \tag{6}$$

Simultaneous solving of Equation (5) and Equation (6) results in Equation (7). Multiply $W_n(x)$ into Equation (7) and integrated according to Equation (8), then we get Equation (9), which $Q_n(t)$ is as stated in Equation (10).

$$m\sum_{n=1}^{\infty}\omega_n^2W_n(x)q_n(t) + m\sum_{n=1}^{\infty}W_n(x)\frac{d^2q_n(t)}{dt^2} + c\sum_{n=1}^{\infty}W_n(x)\frac{dq_n(t)}{dt} + k\sum_{n=1}^{\infty}W_n(x)q_n\,(t) = f(t) \tag{7}$$

$$\int_0^l mW_n^2(x)dx = 1 \tag{8}$$

$$\frac{d^2q_n(t)}{dt^2} + \frac{c}{m}\frac{dq_n(t)}{dt} + \left(\frac{k}{m} + \omega_n^2\right)q_n(t) = Q_n(t) \tag{9}$$

$$Q_{n(t)} = \int_0^l W_n(x)f(t)dx \tag{10}$$

In Equation (9), ω_n is the natural frequency and $\sqrt{\frac{k}{m}}$ is the natural frequency caused by the mooring cable. If the SFT is assumed to be a simple support, its natural frequency is expressed by Equation (11).

$$\omega_n = \left(\frac{n\pi}{l}\right)^2\sqrt{\frac{EI}{m}} + \sqrt{\frac{k}{m}} \tag{11}$$

https://doi.org/10.24191/jmeche.v22i1.4559

Equation (9) is an ordinary differential Equation, so it can be solved numerically. To obtain the $q_n(t)$ solution, the Newmark method is used with parameters $\alpha = 1/6$ and $\beta = 1/2$. Then, the displacement solution is obtained by substituting the value $q_n(t)$ into Equation (3). Based on the displacement solution, the bending moment can be obtained by Equation (12).

$$M(x,t) = EI\frac{\partial^2 w(x,t)}{\partial x^2} \tag{12}$$

The hydrodynamic force

The hydrodynamic force is derived from the kinematics analysis of fluid particles which is formulated using the linear wave theory (Airy theory) (Sumer & Fredsøe, 2006). This theory is used for the ratio of amplitude to wavelength is relatively small. Kinematics analysis of fluid particles begins with determining the potential velocity which is expressed in Equation (13), where H is wave height, k is wave number, z is SFT depth, d is total depth, and T is period of wave.

$$\varphi = \frac{\pi H}{kT}\frac{cosh[k(z+d)]}{sinh(kd)}sin(kx-\omega t) \tag{13}$$

The velocity of the fluid particles can be formulated by deriving Equation (1) in the *x*-axis direction and can be expressed as shown in Equation (13). Furthermore, the acceleration of fluid particles can be obtained by deriving Equation (14) with time (t) as can be seen in Equation (15).

$$\dot{u}_x = \frac{\partial \varphi}{\partial x} = \frac{\pi H}{T}\frac{cosh[k(z+d)]}{sinh(kd)}cos(kx-\omega t) \tag{14}$$

$$\ddot{u}_x = \frac{\partial \dot{u}_x}{\partial t} = \frac{2\pi^2 H}{T^2}\frac{cosh[k(z+d)]}{sinh(kd)}sin(kx-\omega t) \tag{15}$$

The hydrodynamic force is calculated from the component of the drag force and the component of the inertia force which depends on the kinematics equation of the water particles. The hydrodynamic force is usually known as Morison's Equation, as can be seen in Equation (16) (Martire, 2010; Chatjigeorgiou, 2023).

$$f(t) = \frac{1}{2}\rho D C_D \dot{u}|\dot{u}| + \rho A C_I \ddot{u} \tag{16}$$

Here, ρ is the density of the fluid, D is the tunnel diameter, C_D and C_I are the drag and inertia coefficients, respectively. Thus, $\dot{u}$ and $\ddot{u}$ are the velocity and acceleration of the fluid particles, respectively. On the right-hand side of Equation (16), the first term is known as the drag force, while the second term is known as the inertia force. Because the SFT is a floating structure, there is a relative motion between the SFT and the fluid particles, to consider this, the Morisson Equation is modified to Equation (17). Here the subscripts f and s are used to denote the fluid component and the SFT component, respectively. C_m is the additional mass coefficient caused by the mass of the fluid around the moving structure, which can be seen in Equation (18).

$$f(t) = \frac{1}{2}\rho D C_D\left(\dot{u}_f - \dot{u}_s\right)\left|\dot{u}_f - \dot{u}_s\right| + \rho A C_I \ddot{u}_f - \rho A C_m \ddot{u}_s \tag{17}$$

https://doi.org/10.24191/jmeche.v22i1.4559

$$m_a = \rho A C_m \tag{18}$$

Stiffness caused by mooring cable

The configuration of the mooring cables and the diagrams of the forces are shown in Fig 4. The T_0 force exists to balance buoyancy and gravity. The stiffness caused by the mooring cable is influenced by the angle of inclination, the initial stress T_0, the length L_t, the modulus of elasticity E, and the cross-sectional area of cable A. For the inclination angle, $\theta = 0$, the horizontal and vertical stiffnesses are expressed by Equation (19) and Equation (20), respectively.

$$K_h = \frac{2T_0}{L_t} \tag{19}$$

$$K_v = \frac{2EA}{L_t} \tag{20}$$

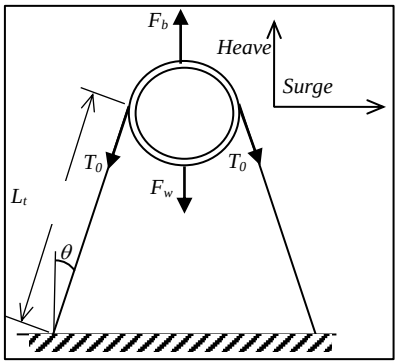

Fig. 4. Configuration of mooring cables and diagrams of forces.

The next discussion is only to determine the stiffness of the horizontal direction (surge). Due to the horizontal movement, the diagram of the forces can be seen in Fig 5. The geometric relationship between angle θ and displacement δ_x can be expressed by Equation (21). If the horizontal stiffness of the SFT is assumed to be a simple spring mechanism, then the Equation for the balance of forces can be expressed as Equation (22).

$$\sin\theta = \frac{\Delta L}{\delta_x} \tag{21}$$

$$K_H \delta_x = (T_0 + \Delta T)\sin\theta - (T_0 - \Delta T)\sin\theta \tag{22}$$

https://doi.org/10.24191/jmeche.v22i1.4559

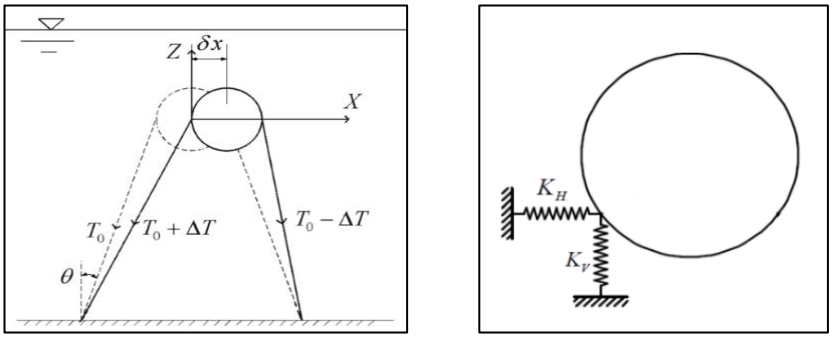

Fig. 5. Horizontal displacement and forces diagram in SFT and the model is assumed to be a simple spring (Frydrýšek et al., 2013).

The mooring cable attached to the SFT, as shown in Fig 6, is modeled as a beam on elastic support (BOES), but it is difficult to obtain an analytical solution. This difficulty was overcome by modeling the SFT as a beam on an elastic foundation (BOEF) (Martire, 2010). The analogy of the BOES model as BOEF shows the suitability of the results and has been verified (Sato et al., 2007; Sato et al. 2008), and the stiffness of the SFT in the horizontal direction can be expressed by Equation (23).

$$K_h = \frac{2AE}{l}\sin^2\theta \tag{23}$$

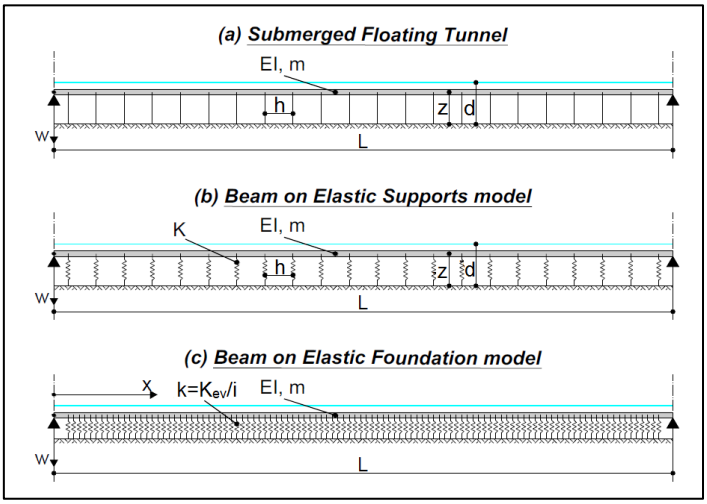

Fig. 6. Analogy of SFT structures: As BOES model and as BOEF model (Martire, 2010).

Verification with finite element method (FEM)

The FEM method converts Equation (2) which is a partial differential equation into an ordinary differential equation, as shown in Equation (24). Here, $[M]$, $[C]$, and $[K]$ are the mass matrix, damping matrix, and stiffness matrix, respectively. Furthermore, $\ddot{\vec{q}}_n$, $\dot{\vec{q}}_n$, and $\vec{q}_n$ are acceleration, velocity, and displacement vectors, respectively. While $\vec{F}$ is a node force vector. This equation can be solved numerically by the Newmark method, by first defining the mass matrix, damping matrix, stiffness matrix, and hydrodynamic force.

https://doi.org/10.24191/jmeche.v22i1.4559

$$[M]\ddot{\vec{q}}_n(t) + [C]\dot{\vec{q}}_n(t) + [K]\vec{q}_n(t) = \vec{F}(t) \tag{24}$$

To represent SFT in FEM, the type of beam element is chosen because it has the same degrees of freedom, namely lateral and rotational directions. The mass matrix is obtained by considering the kinetic energy of the beam elements, which is arranged as Equation (25). Here ρ is the density, A is the cross-sectional area of the tunnel and l is the length of the beam element.

$$[M] = \frac{\rho Al}{420}\begin{bmatrix} 156 & 22l & 54 & -13l \\ 22l & 4l^2 & 13l & -3l^2 \\ 54 & 13l & 156 & -22l \\ -13l & -3l^2 & -22l & 4l^2 \end{bmatrix} \tag{25}$$

SFT stiffness consists of a combination of the tunnel stiffness component and the cable tension component. The tunnel stiffness component is expressed as a bending stiffness matrix. Thus, the SFT stiffness matrix can be arranged as Equation (26) (Frydrýšek et al., 2013; Tiwari & Kuppa, 2014). Here $[K_b]$ is the bending stiffness matrix and$[K_t]$is the cable stiffness matrix, are shown in Equation (27) and Equation (28), respectively. The bending stiffness matrix is obtained by including the strain energy elements of the beam elements, where EI is the bending stiffness.

$$[K] = [K_b] + [K_t] \tag{26}$$

$$[K_b] = \frac{EI}{l^3}\begin{bmatrix} 12 & 6l & -12 & 6l \\ 6l & 4l^2 & -6l & 2l^2 \\ -12 & -6l & 12 & -6l \\ 6l & 2l^2 & -6l & 4l^2 \end{bmatrix} \tag{27}$$

Meanwhile, the stiffness matrix due to the mooring cables, $[K_t]$, is obtained by assuming the SFT as the beam on the elastic foundation (BOEF). Under the BOEF assumption, the stiffness of the mooring cable is distributed evenly along the SFT and is equivalent to its original condition (Sato et al., 2008).

$$[K_t] = \begin{bmatrix} 13lk/35 & 11l^2k/210 & 9lk/70 & -13l^2k/420 \\ 11l^2k/210 & l^3k/105 & 13l^2k/420 & -l^3k/140 \\ 9lk/70 & 13l^2k/420 & 13lk/35 & -11l^2k/210 \\ -13l^2k/420 & -l^3k/140 & -11l^2k/210 & l^3k/105 \end{bmatrix} \tag{28}$$

The fluid around the SFT causes a viscous attenuation. In the present study, viscous damping is calculated as structural damping. Some studies assume an attenuation ratio of 0.25% (Muhammad et al., 2017; Long et al., 2009). The damping matrix can be constructed based on the Rayleigh method, as stated in Equation (29). Here α and β are constants that are affected by the damping ratio and natural frequency. If the damping ratio of the two vibrating modes is assumed to be the same $(\zeta_i = \zeta_j)$, then the α and β values are obtained from Equations (30) and (31), respectively.

$$[C] = \alpha[M] = \beta[K] \tag{29}$$

$$\alpha = \zeta\frac{2\omega_i\omega_j}{\omega_i + \omega_j} \tag{30}$$

https://doi.org/10.24191/jmeche.v22i1.4559

$$\beta = \zeta \frac{2}{\omega_i + \omega_j} \tag{31}$$

In FEM analysis, the distributed force is converted into a force vector at each node. The forces at the nodes must be equivalent to the distributed forces. This is done by multiplying the distributed force $f(x,t)$ and the function matrix of the form $[N(x)]^T$ and then integrating it along the elements, as shown in Equation (32).

$$\vec{F}(t) = \int_0^l [N(x)]^T \, \mathrm{f}(x,t) dx \tag{32}$$

Numerical example

As a case example, the present study analyzed the SFT prototype model in Qiandao Lake, China (Mazzolani & Barbella, 2008; Muhammad et al., 2017), with modifications to the configuration of the mooring cable, as shown in Fig 7. The values of the design parameters can be seen in Table 1, Table 2, and Table 3.

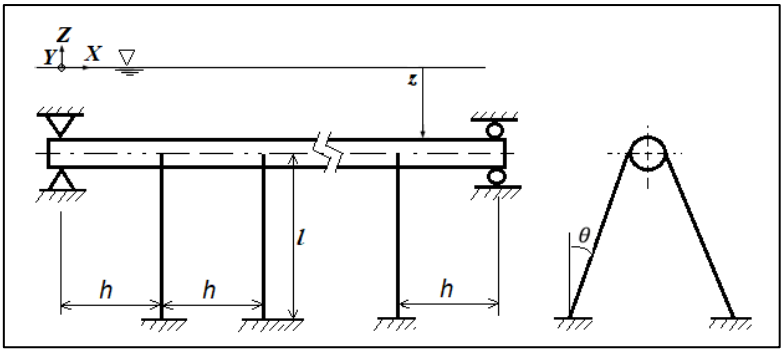

Fig. 7. Example model.

Table 1. Tunnel's parameters

Parameter	Unit	Value
Length	m	100
Area	m^2	5.1
Moment of inertia	m^4	12.3
Specific mass	kg/m^4	2451
Elasticity	N/m^2	$3x10^{10}$

https://doi.org/10.24191/jmeche.v22i1.4559

Table 2. Mooring cable parameters

Parameter	Unit	Value
Diameter	m	0.06
Density	kg/m^3	7850
Moment of inertia	m^4	$6x10^7$
Modulus of elasticity	N/m^2	$1.4x10^{11}$
The angle of inclination of the mooring cables	degree°	0
		15
		30
		45
Distance between mooring cables	m	15
		20
		25
		30

Table 3. Wave parameters

Parameter	Unit	Value
Wave height	m	1
Wave period	s	2.3
Depth levels	m	30
Water density	kg/m^3	1050
Drag coefficient		1
Inertia coefficient		2
SFT position depth level	m	2
		5
		10

RESULTS AND DISCUSSION

This section discusses the accuracy of the results of the MSM analysis compared to FEM. Furthermore, a study of the influence of the design parameters on the dynamic behavior of the SFT is presented.

Modal analysis: DI-MSM to FEM results comparison

Fig 8 shows the first four vibration modes and a comparison between FEM and DI-MSM. Here, it can be seen at the initial vibration mode that the two methods give results that are in agreement, but are increasingly different from the subsequent vibration modes. This is due to the relatively small number of elements used in the FEM (only 10 beam elements). To obtain more accurate results, using FEM requires a larger number of elements with relatively expensive computational costs (Rao, 2017b), but using DI-MSM is relatively cheaper because it is an analytical process.

The comparison of natural frequencies between DI-MSM and FEM can be seen in Fig 9. Here it can be seen that in the initial vibration mode, it is known that the natural frequencies between DI-MSM and FEM are relatively the same, but from the 10^{th} natural frequency, there is a significant difference. This means that the dynamic behavior of SFT can be represented by FEM only at low frequencies. On the other hand, DI-MSM can be used both in low-vibration mode and high-vibration mode.

https://doi.org/10.24191/jmeche.v22i1.4559

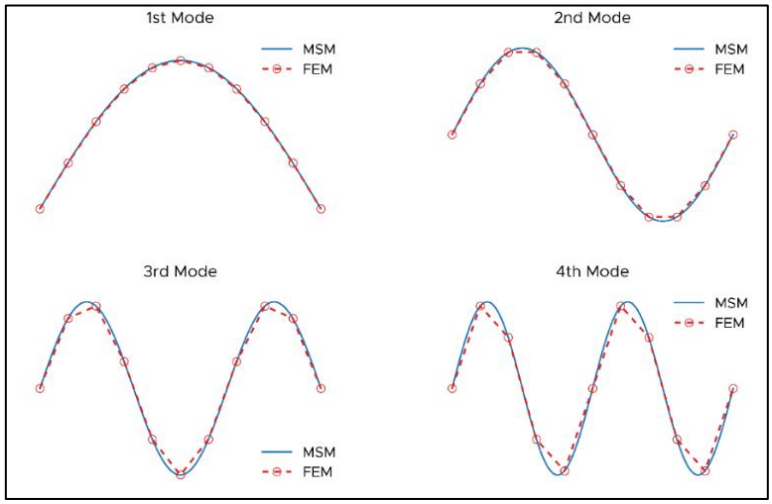

Fig. 8. Vibration mode: DI-MSM and FEM comparison.

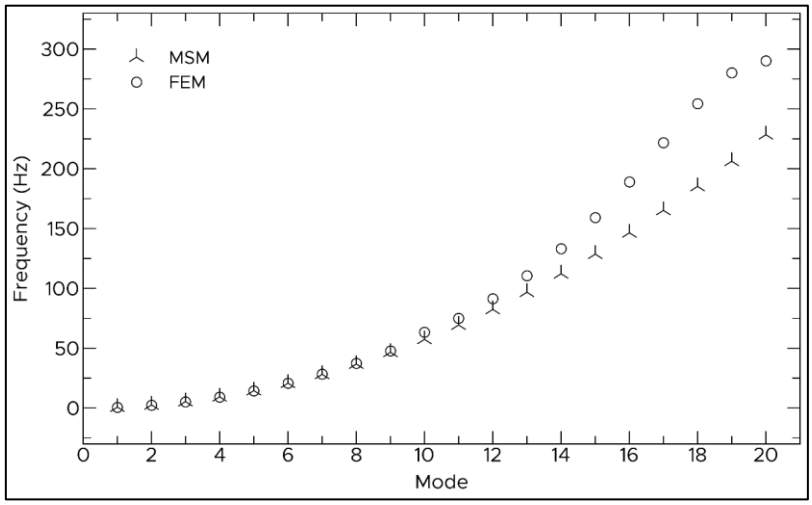

Fig. 9. Natural frequencies: DI-MSM and FEM comparison.

Hydrodynamic force

The hydrodynamic forces were calculated according to Table 3, using the Morison equation. The hydrodynamic force distributed along the SFT, using the FEM is converted into a force at the nodes according to Equation (32). Force During the numerical simulation process using the FEM, the distributed force is converted into a nodal force. Fig 10 shows the hydrodynamic forces acting on the SFT. Hydrodynamic forces consist of two components: inertia forces which are relatively very large when compared to drag forces with an amplitude ratio of 0.0055. The dominance of the inertia force is caused by the relatively large ratio of SFT diameter to wavelength (ratio $D/\lambda = 0.69$). This statement is in accordance with previous studies that if $D/\lambda > 0.2$ then the inertia force component is more dominant and the diffraction effect can be ignored (Sundar, 2016).

https://doi.org/10.24191/jmeche.v22i1.4559

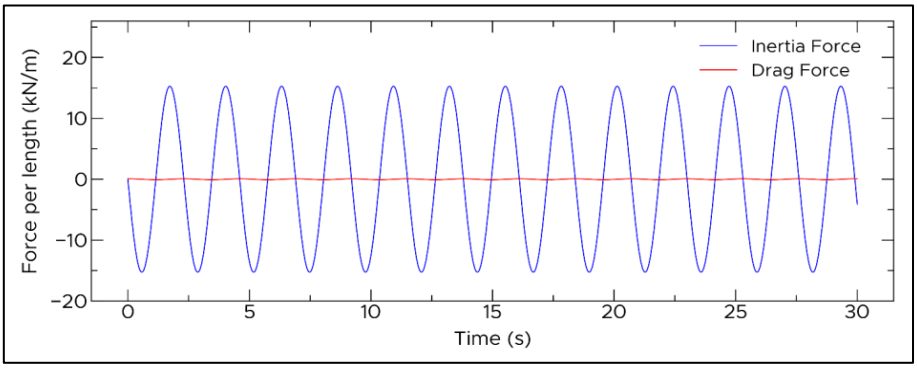

Fig. 10. Hydrodynamic force.

Displacement

Fig 11 shows the displacement of the SFT in the midspan horizontal position, a comparison between using the FEM and using the MSM. Displacement is displayed for 30 seconds during the loading process. The comparison of the displacement amplitudes in the first 10 values and their differences are shown in Table 4, where it can be seen that using the MSM and FEM will produce an agreement solution. This result also agrees with the research of Muhammad et al. (2017).

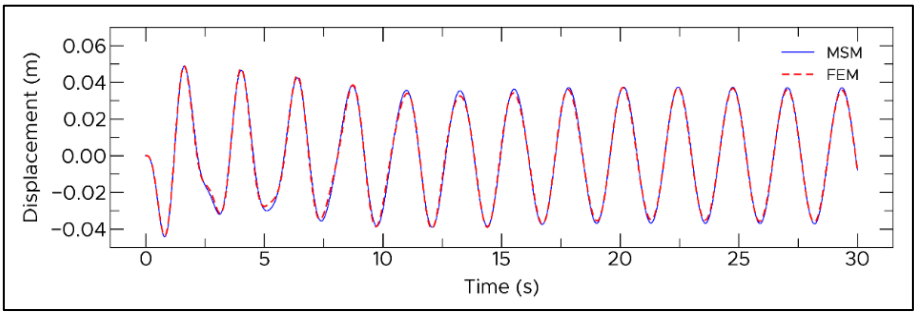

Fig. 11. Midspan displacement: DI-MSM vs FEM.

Table 4. Peak Displacement Value: DI-MSM and FEM comparison

Peak of	Using FEM (m)	Using MSM (m)	Differences (%)
1	0.0488	0.0489	0.17
2	0.0475	0.0465	2.19
3	0.0436	0.0424	2.83
4	0.0385	0.0383	0.66
5	0.0340	0.0356	4.60
6	0.0325	0.0353	7.96
7	0.0342	0.0362	5.72
8	0.0361	0.0371	2.68
9	0.0371	0.0374	0.96
10	0.0371	0.0374	0.74

https://doi.org/10.24191/jmeche.v22i1.4559

Parametric studies

In this section, the influence of parameters on the dynamic behavior of SFT will be discussed, including; the level of installation depth, the slope of the mooring cable, the distance between the mooring cables, and the bending moment in the SFT midspan.

The effect of depth level on displacement

The depth level of the SFT installation affects the hydrodynamic forces that work and also affects the displacement that occurs. Fig 12 shows the displacement of the SFT at a depth of 2 m, 5 m, and 10 m below the water surface. Here it can be seen that the SFT installed on the water surface has the largest displacement, and gets smaller at higher depth levels. This is due to the kinematics of fluid particles at the water surface having a much greater speed and acceleration compared to deeper positions, as stated in Equation (14), Equation (15), and Fig 13, which are also in agreement with the results of the study Chen et al. (2018) and Paik & Chang (2004). Based on this phenomenon, it can be suggested that the position of the SFT installation should consider the optimal depth level, on the one hand, to avoid the position of the water surface and on the other hand, it is necessary to avoid large hydrostatic pressure.

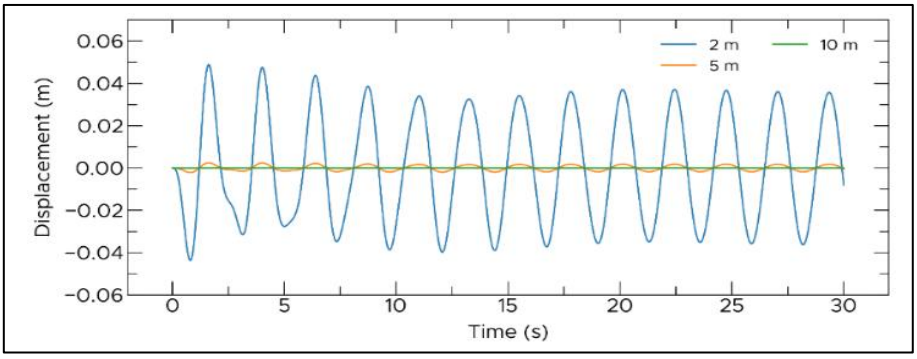

Fig. 12. Effect of depth level on midspan displacement.

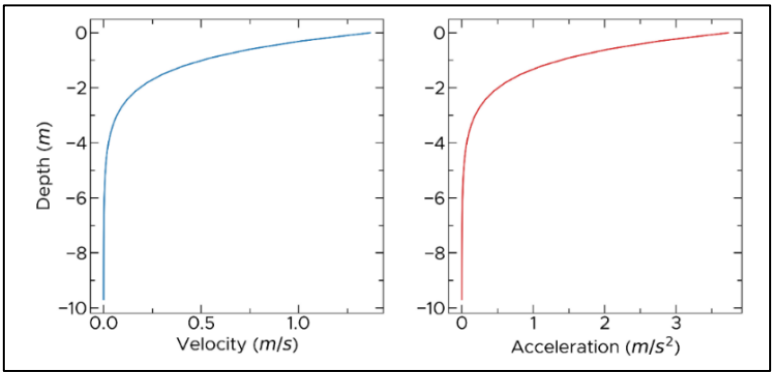

Fig. 13. Fluid particle kinematics at various depth levels.

The effect of the slope angle and mooring cable distance on displacement

The slope of the mooring cable affects the stability of the SFT structure. In this study, the slope of the mooring cable was varied from 0° to 45° and the SFT displacement for 30 seconds of loading for each

https://doi.org/10.24191/jmeche.v22i1.4559

variation is shown in Fig 14(a). From the picture, it can be seen that SFT without the slope of the mooring cable has the largest displacement. Meanwhile, SFT with the slope of mooring cable (45°) has the smallest displacement. It can be stated that the greater the slope angle of the mooring cable, the smaller the SFT displacement will be. The slope of the mooring cable affects its stiffness, as stated in Equation (23), as well as affects its displacement (Chen et al., 2018; Lin et al., 2018; Long et al., 2009).

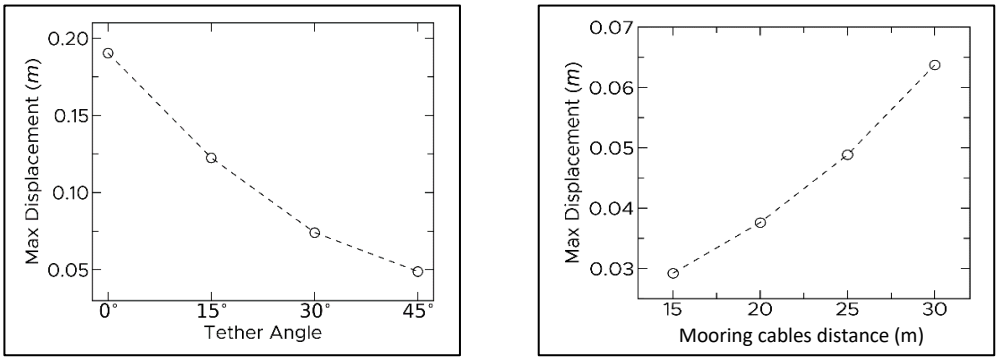

Fig. 14. Effect of (a) slope angle of mooring cables, and (b) mooring cables distance.

The effect of the mooring cable distance on midspan displacement is shown in Fig 14(b). In this study, the mooring cables distance were varied by 15 m, 20 m, 25 m, and 30 m. It can be seen that the smaller the distance between the mooring cables, the smaller the SFT displacement.

Bending moment

The bending moment of the SFT structure can be obtained from Equation (12) and is shown in Fig 15. Based on the Euler-Bernoulli beam theory, positive bending moments and negative bending moments are generated due to dynamic loading. If the damping factor is neglected, the dynamic bending moment is relatively larger than the static bending moment. On the other hand, if the damping factor is included, the dynamic bending moment is relatively smaller than the static bending moment, this is consistent with previous research (Muhammad et al., 2017).

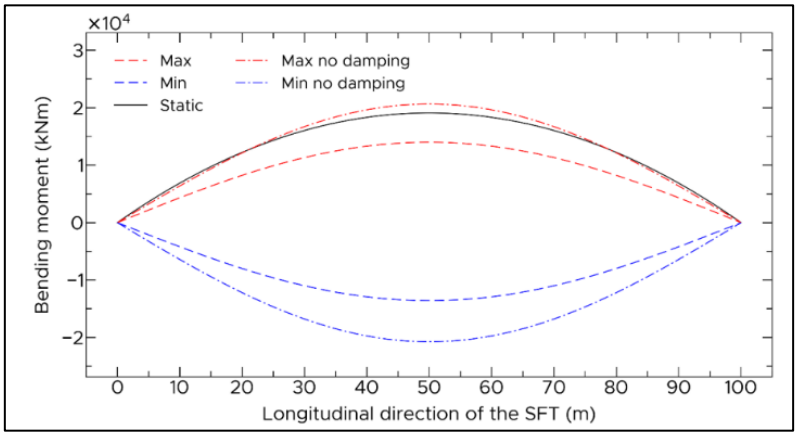

Fig. 15. Comparison of static and dynamic moments.

https://doi.org/10.24191/jmeche.v22i1.4559

In order to assess the validity of the calculation results, calculations are needed with examples available in the literature. The same FEM method has been used to analyze the dynamics of the SFT prototype in Qiandao Lake, China. The maximum static bending moment at midspan can be seen in Table 5. The relative differences are caused by the present study, the mooring cable is modeled using a beam on an elastic foundation (BOEF) which causes the stiffness of the mooring cable to be evenly distributed throughout the tunnel.

Table 5. Maximum static bending moment at midspan

	Present study	Mazzolini et al [12]	Muhammad et al [5]
Max. bending (kN.m)	16.1	17.0	13.7
Differences (%)		5.3	17.5

CONCLUSION

The Direct Integration-Mode Superposition Method (DI-MSM) which is applied to study the dynamic response of the SFT model has high accuracy when compared to the FEM and compared to several previous studies. This can be seen in the studies conducted, including the vibration mode, natural frequency, hydrodynamic force, displacement, and moment in the midspan. One of the advantages of using the DI-MSM is that the solution can be obtained analytically, which is simpler when compared to FEM. With simpler steps, parametric studies can easily be carried out for design needs. In this research, a parametric study was conducted to see the effect of the SFT depth level, the effect of the slope of the mooring cable, and the effect of the distance between the mooring cables. The higher the SFT depth level, the smaller the wave force, displacement, and bending moment. Furthermore, the greater the slope angle of the mooring cable results in a smaller displacement. The distance between the mooring cables also affects the displacement that occurs.

ACKNOWLEDGEMENTS/FUNDING

The authors would like to acknowledge the support of the Institute for Research and Community Service, University of Lampung, Indonesia, for providing the facilities and financial support for this research, under the basic research scheme, SPK No. 669/UN26.21/PN/2023, dated April 10, 2023.

CONFLICT OF INTEREST STATEMENT

The authors agree that this research was conducted in the absence of any self-benefits, commercial, or financial conflicts and declare the absence of conflicting interests with the funders.

AUTHORS' CONTRIBUTIONS

The authors confirm their contribution to the paper as follows: **Study conception and design, Supervision, review & editing**: Jamiatul Akmal; **Numerical analysis, writing – original draft**: Nurcahya Nugraha; **Analysis and interpretation of results**: Asnawi Lubis; **Draft manuscript preparation**: Martinus. All authors reviewed the results and approved the final version of the manuscript.

https://doi.org/10.24191/jmeche.v22i1.4559

REFERENCES

Akgün, M. A. (1993). A new family of mode-superposition methods for response calculations. Journal of Sound and Vibration, 167(2), 289–302.

Bathe, K. J. (2014). Finite element procedures. (2nd Ed.). Prentice Hall.

Blaszczyk, T. (2017). Analytical and numerical solution of the fractional Euler–Bernoulli beam equation. Journal of Mechanics of Materials and Structures, 12(1), 23–34. https://doi.org/10.2140/jomms.2017.12.23

Chatjigeorgiou, I. K. (2023). Dynamic behavior of pipelines for marine applications. Distributed Forces—Hydrodynamic Loads (pp. 45–70). Springer International Publishing.

Chen, Z., Xiang, Y., Lin, H., & Yang, Y. (2018). Coupled vibration analysis of submerged floating tunnel system in wave and current. Applied Sciences, 8(8), 1311. https://doi.org/10.3390/app8081311

Ereiz, S., Duvnjak, I., & Jimenez-Alonso, J. F. (2021). Finite element model updating methods for structural application. Proceedings of the 32nd DAAAM International Symposium (pp. 712-718). DAAAM International. https://doi.org/10.2507/32nd.daaam.proceedings.099

Ereiz, S., Duvnjak, I., & Jiménez-Alonso, J. F. (2022). Review of finite element model updating methods for structural applications. Structures, 41(1), 684–723. https://doi.org/10.1016/j.istruc.2022.05.041

Frydrýšek, K., Jančo, R., & Gondek, H. (2013). Solutions of beams, frames and 3D structures on elastic foundation using FEM. International Journal of Mechanics, 7(4), 362-369.

Jin, C., & Kim, M. (2021). The effect of key design parameters on the global performance of submerged floating tunnel under target wave and earthquake excitations. Computer Modeling in Engineering & Sciences, 128(1), 315–337. https://doi.org/10.32604/cmes.2021.016494

Jin, C., & Kim, M. H. (2018). Time-Domain hydro-elastic analysis of a SFT (submerged floating tunnel) with Mooring Lines under extreme wave and seismic excitations. Applied Sciences, 8(12), 2386. https://doi.org/10.3390/app8122386

Kocakaplan, S., & Tassoulas, J. L. (2019). Wave propagation in initially-stressed elastic rods. Journal of Sound and Vibration, 443, 293–309. https://doi.org/10.1016/j.jsv.2018.11.045

Lin, H., Xiang, Y., & Yang, Y. (2019). Vehicle-tunnel coupled vibration analysis of submerged floating tunnel due to tether parametric excitation. Marine Structures, 67, 102646. https://doi.org/10.1016/j.marstruc.2019.102646

Lin, H., Xiang, Y., Yang, Y., & Chen, Z. (2018). Dynamic response analysis for submerged floating tunnel due to fluid-vehicle-tunnel interaction. Ocean Engineering, 166, 290–301. https://doi.org/10.1016/j.oceaneng.2018.08.023

Long, X., Ge, F., Wang, L., & Hong, Y. (2009). Effects of fundamental structure parameters on dynamic responses of submerged floating tunnel under hydrodynamic loads. Acta Mechanica Sinica, 25(3), 335–344. https://doi.org/10.1007/s10409-009-0233-y

Maqbul, Md., & Gupta, N. (2021). Approximate solutions to Euler–Bernoulli beam type equation. Mediterranean Journal of Mathematics, 18, 196. https://doi.org/10.1007/s00009-021-01833-2

Martinelli, L., Barbella, G., & Feriani, A. (2011). A numerical procedure for simulating the multi-support seismic response of submerged floating tunnels anchored by cables. Engineering Structures, 33(10),

https://doi.org/10.24191/jmeche.v22i1.4559

2850–2860. https://doi.org/10.1016/j.engstruct.2011.06.009

Martire, G. (2010). The development of submerged floating tunnels as an innovative solution for waterway crossings. [Doctoral dissertation, Università degli Studi di Napoli Federico II]. Retrieved from http://www.fedoa.unina.it/8407/.

Martire, G., Faggiano, B., & Mazzolani, F. M. (2010). Compared cost evaluation among traditional versus innovative strait crossing solutions. Procedia Engineering, 4, 293–301. https://doi.org/10.1016/j.proeng.2010.08.033

Mazzolani, F. M., Landolfo, R., Faggiano, B., Esposto, M., Perotti, F., & Barbella, G. (2008). Structural analyses of the submerged floating tunnel prototype in Qiandao Lake (PR of China). Advances in Structural Engineering, 11(4), 439–454. https://doi.org/10.1260/136943308785836862

Minoretti, A., Myhr, A., Haugerud, S. A., Sekse, J., & Egeberg, T. F. (2016). The submerged floating tube bridge: The invisible bridge crossing the Bjørnafjord. International Association for Bridge and Structural Engineering Congress (pp. 1875–1882). IABSE Publishing.

Muhammad, N., Ullah, Z., & Choi, D. H. (2017). Performance evaluation of submerged floating tunnel subjected to hydrodynamic and seismic excitations. Applied Sciences, 7(11), 1122. https://doi.org/10.3390/app7111122

Paik, I. Y., Oh, C. K., Kwon, J.S., & Chang, S. P. (2004). Analysis of wave force induced dynamic response of submerged floating tunnel. KSCE Journal of Civil Engineering, 8(5), 543–550.

Rao, S. S. (2017). Mechanical vibrations. (6th Ed.). Pearson Education.

Rao, S. S. (2017). The finite element method in engineering. (6th Ed.). Elsevier.

Remseth, S. N., Leira, B. J., Okstad, K. M., Mathisen, K. M., & Haukås, T. (1999). Dynamic response and Fluid/Structure interaction of submerged floating tunnels. Computer and Structures, 72(4-5), 659–685.

Sato, M., Kanie, S., & Mikami, T. (2007). Structural modeling of beams on elastic foundations with elasticity couplings. Mechanics Research Communications, 34(5–6), 451–459. https://doi.org/10.1016/j.mechrescom.2007.04.001

Sato, M., Kanie, S., & Mikami, T. (2008). Mathematical analogy of a beam on elastic supports as a beam on elastic foundation. Applied Mathematical Modelling, 32(5), 688–699. https://doi.org/10.1016/j.apm.2007.02.002

Sorokin, S. V., Broberg, P. H., Steffensen, M. T., & Ledet, L. S. (2022). Finite element modal analysis of wave propagation in homogeneous and periodic waveguides. International Journal of Mechanical Sciences, 227, 107444. https://doi.org/10.1016/j.ijmecsci.2022.107444

Sumer, B. M., & Fredsøe, J. (2006). Hydrodynamics around cylindrical structures. (Revised Ed.). World Scientific Publishing.

Sundar, V. (2016). Ocean wave mechanics: Applications in Marine Structures. John Wiley & Sons.

Tang, S.Q., & Karpov, E. G. (2014). Artificial boundary conditions for Euler-Bernoulli beam equation. Acta Mechanica Sinica, 30(5), 687–692. https://doi.org/10.1007/s10409-014-0089-7

Tariverdilo, S., Mirzapour, J., Shahmardani, M., Shabani, R., & Gheyretmand, C. (2011). Vibration of submerged floating tunnels due to moving loads. Applied Mathematical Modelling, 35(11), 5413-5425. https://doi.org/10.1016/j.apm.2011.04.038

https://doi.org/10.24191/jmeche.v22i1.4559

Thomson, W. T. (2018). Theory of vibration with applications. (1st Ed.). CrC Press.

Tiwari, K., & Kuppa, R. (2014). Overview of methods of analysis of beams on elastic foundation. IOSR Journal of Mechanical and Civil Engineering, 11(5), 22–29.

Xiang, Y., Lin, H., Bai, B., Chen, Z., & Yang, Y. (2021). Numerical simulation and experimental study of submerged floating tunnel subjected to moving vehicle load. Ocean Engineering, 235(6), 109431. https://doi.org/10.1016/j.oceaneng.2021.109431

Xiong, M., Chen, Z., & Huang, Y. (2023). Nonlinear stochastic seismic dynamic response analysis of submerged floating tunnel subjected to non-stationary ground motion. International Journal of Non-Linear Mechanics, 148(12), 104270. https://doi.org/10.1016/j.ijnonlinmec.2022.104270

Yu, M., Nie, X., Yang, G., & Zhong, P. (2020). Fixed-point fluid structure interaction analysis based on geometrically exact approach. Scientific Reports, 10(1), 10322. https://doi.org/10.1038/s41598-020-66854-5

Yuan, Z., Man-sheng, D., Hao, D., & Long-chang, Y. (2016). Displacement response of submerged floating tunnel tube due to single moving load. Procedia Engineering, 166, 143–151. https://doi.org/10.1016/j.proeng.2016.11.577

https://doi.org/10.24191/jmeche.v22i1.4559